Est. 1841 | YORK ST JOHN UNIVERSITY

Xiao, Xiao, Zhao, Hui, Li, Lin-Feng, Qu, Bing-Liang, Wu, Yu-Lian, Zhu, Yin-Ling, Chen, Bei-Bei and Pan, Gang (2023) Ion exchange coupled biomineral self-sacrificial template synthesis of N-enriched porous carbon as robust electrocatalyst for rechargeable Zn-air battery. Rare Metals, 42. pp. 1186-1194.

Downloaded from: https://ray.yorksj.ac.uk/id/eprint/7371/

The version presented here may differ from the published version or version of record. If you intend to cite from the work you are advised to consult the publisher's version: http://dx.doi.org/10.1007/s12598-022-02190-z

Research at York St John (RaY) is an institutional repository. It supports the principles of open access by making the research outputs of the University available in digital form. Copyright of the items stored in RaY reside with the authors and/or other copyright owners. Users may access full text items free of charge, and may download a copy for private study or non-commercial research. For further reuse terms, see licence terms governing individual outputs. Institutional Repositories Policy Statement

RaY

Research at the University of York St John

For more information please contact RaY at ray@yorksj.ac.uk

Ion exchange coupled biomineral self-sacrificial template synthesis of N-enriched porous carbon as robust electrocatalyst for rechargeable Zn-air battery

Xiao Xiao, Hui Zhao, Lin-Feng Li, Bing-Liang Qu, Yu-Lian Wu, Yin-Ling Zhu,
Bei-Bei Chen*, Gang Pan*
X. Xiao, H. Zhao, L.-F. Li, B.-L. Qu, Y.-L. Wu, Y.-L. Zhu
School of Chemistry and Environment, Guangdong Ocean University, Zhanjiang 524088, PR China
X. Xiao, H. Zhao, L.-F. Li, B.-L. Qu, G. Pan**
Research Center for Coastal Environmental Protection and Ecological Resilience, Guangdong Ocean University, Zhanjiang 524088, PR China
gang.pan@ntu.ac.uk
B.-B. Chen*
College of Coastal Agricultural Science, Guangdong Ocean University, Zhanjiang 524088, PR China
beibeichenk@outlook.com
G. Pan**
School of Humanities, York St John University, Lord Mayor's Walk, York, YO31 7EX, United Kingdom

Abstract To realize the commercialize of rechargeable Zn-air battery (RZAB), developing metal-free bifunctional electrocatalysts with satisfactory activity for ORR (oxygen reduction reaction) and OER (oxygen evolution reaction) is one of the emerging issues. Herein, a prawn shells-derived N-enriched porous carbon (PSNC) is synthesized via an ion exchange coupled biomimetic self-sacrificing template strategy. The resulting PSNC displays unique functional components, including the interconnected macro-meso-micropores structure to shorten charge and mass transfer pathway, high content of pyridinic and graphitic nitrogen to construct rich catalytic active site and improve conductivity. As electrocatalysts in alkaline condition, the optimized PSNC-0.8 achieves excellent bifunctional catalytic propriety with a narrow potential gap (ΔE) value of 0.80 V. Meanwhile, PSNC-0.8 based RZAB displays a high peak power density of 176.5 $mW \cdot cm^{-2}$ and considerable cycling durability with a small battery efficiency delay of 6.5% after 480 cycles (320 h). This study enlightens a simple and effective conception to design high performance metal-free bifunctional electrocatalysts from seafood waste.

Keywords Rechargeable Zn-air battery (RZAB); Bifunctional electrocatalyst; N-enriched porous carbon; Biomineral self-sacrificial template; Ion exchange

1 Introduction

With the increasing demands of energy and environmental sustainability, extensive attention has been focused on the renewable and clean energy [1-5]. Consequently, exploiting the high energy density storage and conversion system has become an inevitable choice [6-11]. Among these systems, rechargeable Zn-air battery (RZAB) displays tremendous application foreground due to various merits, including the eco-friendly, low-cost and high energy density [12-14]. However, the electrochemical performance of RZAB is primarily limited by the sluggish ORR (oxygen reduction reaction) and OER (oxygen evolution reaction) dynamics process [15-17]. The noble metal-based catalysts, such as Pt/C or RuO_2, exhibit well ORR or OER catalytic activity [18]. But their large-scale application is still subject to the scarcity nature and insufficient bifunctional catalytic properties.

Up to now, the heteroatom-doped porous carbon materials (HPCMs) have been widely regards as the one of the most promising electrocatalysts for RZAB considering their high surface area, environmental acceptability, high electric conductivity and excellent catalytic performance, as well as considerable

stability [19]. The theoretical calculations and experimental studies have demonstrated that the heteroatom (e.g. N, S, P) can effectively improve the oxygen catalytic activity of carbon [20-22]. For N-doped carbon, the higher electronegativity of N can change the surface charge distribution of C atoms, which can create rich catalytic active sites and form strong N-C bonds [23]. Specially, the graphitic-N and pyridinic-N (i.e., C-N bonding as active sites) are believed to play a crucial key role in improving ORR and OER process because of the enhanced π bonding [24]. Besides, the porosity of carbon material also plays a vital role in enhancing oxygen catalytic activity [25]. Particularly constructing a macro-meso-micropores structure in carbon material is an effective strategy to reduce O_2 and electrolyte diffusion and mass-transfer resistance [26,27]. Meanwhile, the above hierarchical porous structure can largely expose the catalytic sites for oxygen conversion. Hard templates strategy is one of the most popular methods for synthesizing HPCMs [28-30]. For instance, colloidal silica particles have been widely adopted as template for ordered mesopore carbon [31,32]. But the removal of silica template is environmentally unfriendly because of the corrosive HF or concentrated alkali solution. For comparison, some biomineral materials, such as $CaCO_3$, have been considered as a more suitable option because of the well-tunable morphology, greenness, and simplicity of removing templates [33]. In addition, the pyrolysis ash (CaO) can also play a role in regulating pore structure. Significantly, the uniform dispersion and content of $CaCO_3$ can largely affect the distribution of pore structure and N atom. Therefore, how to maintain the uniform dispersion and accurate content of $CaCO_3$ is an essential issue needed to address to construct high-performance HPCMs electrocatalyst.

Ingeniously, some seafood waste (e.g. prawn shells) possesses unique component characteristics [34,35]. In the natural condition, $CaCO_3$ component is evenly distributed in prawn shells to maintain the stability of shell structure. And edetate disodium (EDTA-2Na) solution can be used as an ion exchanger to precise regulate the content of $CaCO_3$ via the strong coordination between EDTA-2Na and Ca^{2+}. Additionally, prawn shells are also rich in protein and chitin, which can be served as nitrogen source [36]. According to the above discussion, it can enlighten that the prawn shells can be served as a fine and cheap precursor of HPCMs, and then synchronously realize the uniform design of pore structure and N-doping. Furthermore, as an abundant and cheap renewable resource, the prawn shells is mainly treated by sanitary landfill [37]. The resource utilization rate of prawn shells is far from satisfactory. Hence, exploring the potential application of prawn shells waste in the field of electrocatalysis may be a viable option.

In this work, we introduce an ion exchange coupled biomineral self-sacrificing template approach to precisely design prawn shells-derived N-enriched porous carbon (PSNC) as an effective metal-free bifunctional electrocatalyst for RAZB. The resulting PSNC samples possess unique structural characteristics, including interconnected macro-meso-micropores structure distribution to provides a high infiltrated area to fully exposed catalytic active site and shorten O_2 and electrolyte diffusion pathway, the high content of pyridinic-N and graphitic-N to construct rich catalytic active site to strengthen the catalytic activity as well as optimize the charge transfer. As a bifunctional electrocatalyst, the optimized PSNC-0.8 displays excellent ORR/OER catalytic activity, and the PSNC-0.8 based RZAB displays a high peak power density and considerable cycling stability.

2 Experimental

2.1 Material synthesis

The synthesis process of PSNC is described as follows: 5 g pre-dried prawn shells powder (300 mesh)

was dispersed into 100 ml EDTA-2Na aqueous solution with an aqueous solution concentration range (0-0.15 mol·L^{-1}) to remove $CaCO_3$ partly. After stirring for 0.5 h, the filter residue was rinsed with deionized H_2O and then freeze-dired. Subsequently, the obtained filter residue was transferred to a pyrolysis furnace to anneal at 750 °C for 2 h (Ar, 5 °C·min^{-1}). After that, the product was further purified by HCl solution (0.5 mol·L^{-1}) to obtain the PSNC sample. According to the percentage of $CaCO_3$ in filter residue, the as-made PSNC samples were named PSNC-0.2, PSNC-0.5, PSNC-0.8 and PSNC-1.0.

2.2 Apparatus/Instrumentation

The morphological structures analysis was performed by FEI Tecnai G2 F20 transmission electron microscopy (TEM) and Zeiss SIGMA 300 scanning electron microscopy (SEM). The crystal structure of as-made sample was studied by X'Pert Pro MPD X-ray diffraction (XRD, λ=0.154056 nm, Cu Kα radiation) and LabRAM HR Evolution Raman spectroscopy (532 nm). The N_2 adsorption-desorption test was carried out on a Micromeritics ASAP 2020 instrument. XPS spectrometer (Thermo ESCALAB 250X) was used to analyze the binding environments of elements.

2.3 Electrochemical measurement

All the electrochemical tests were carried out via three-electrode cell design, including an Al_2O_3-polished glass carbon electrode (GC disk area: 0.196 cm^2) loaded catalyst ink as working electrode, a platinum wire as counter electrode and a Hg/HgO electrode (1 mol^{-1}·L KOH) as reference electrode. The ORR measurements were performed in 0.1 mol·L^{-1} O_2/N_2-saturated KOH solution, while OER measurements were carried out in N_2-saturated KOH solution. And the scan rate was kept at 5 mV·s^{-1} for linear sweep voltammetry (LSV). Additionally, the current-time (*i-t*) chronoamperometric measurement was also conducted to evaluate the durability of catalyst. It is worth noting that all the potential values were quoted versus RHE by the equation: E(RHE)= E(Hg/HgO) + 0.059×pH + 0.098, and the current density was calculated to the geometric area of working electrode.

The working electrode was prepared as follows: firstly, 5 mg catalyst power was dispersed into water and 1 ml 1:1 (volume ratio) water/ethanol solvent containing 50 μl Nafion solution (5%) and ultrasonicated for 60 min to formed a homogenous ink. Secondly, 10 μl ink was dropped on the Al_2O_3-polished glass carbon electrode surface and then natural drying to form the working electrode with a catalyst loading of 0.256 mg·cm^{-2}.

A homemade Zn-air cell was assembled to further demonstrate the bifunctional catalytic activity of as-made sample with the Pt/C+RuO_2 as the reference. Typically, the air electrode was comprised of nickel screen with a catalyst layer and a gas-diffusion layer. A polished Zn plate and mix solution (6 mol·L^{-1} KOH+ 0.2 mol·L^{-1} $Zn(CH_3COO)_2$) were served as the anode and electrolyte, respectively. A LAND CT2001A testing station was used to measure the cycling reversibility and discharge performance with the current density of 10 mA·cm^{-2}. The discharge-charge polarization data was collected by a CHI660 electrochemical working station. All the performance tests were conducted at room temperature, and the detailed tests process was given in our previous publication [14, 35].

3 Results and discussion

3.1 Physical characterization of PSNC samples

The fabrication procedures of PSNC sample are illustrated in Fig. 1a. Before the pyrolysis process, the content of $CaCO_3$ of prawn shells is first precisely regulated by virtue of the strong coordination between EDTA-2Na and Ca^{2+}. During the pyrolysis process, the residual $CaCO_3$ component is used as the hard template and pore-forming material to regulate the pore structure distribution. Meanwhile, the in-situ N-

doping was realized by the nitrogen rich components (chitin and protein). Then the ash was removed by HCl solution, the PSNC sample is successfully synthesized.

From XRD patterns in Fig. 1b, all four PSNC samples display two broad characteristic diffraction peaks at 25° and 43°, which are related to (002) and (100) planes of carbon material [38]. In addition, Raman spectra of PSNC samples exhibit two distinct peaks (Fig. 1c). One peak located ~1340 cm^{-1} belongs to D band for the disordered carbon atoms, and the other peak at ~1580 cm^{-1} corresponds to G band for graphitic carbon [39,40]. The defective degree of carbon material can be evaluated by intensity ratios (I_G/I_D). In general, a smaller I_G/I_D value tend to display more defects and disorders. PSNC-0.8 exhibits a smaller I_G/I_D value of 0.514 than other PSNC samples. This represents more defects and disorders are existed in PSNC-0.8, which are favorable for accelerating the oxygen electrocatalytic process. Besides, Nitrogen sorption measurement of PSNC samples deliver a pronounced hysteresis loop at relative pressure (P/P_0) >0.45 (Fig. 1d), indicating the typical mesoporous nature [41]. Meanwhile, a distinct nitrogen uptake also observed at P/P_0 <0.1, implying the existence of micropore structure. Furthermore, comparing with other PSNC samples (Table S1), PSNC-0.8 delivers the largest BET surface area and total pore volume of 395.7 $m^2 \cdot g^{-1}$ and 0.413 $cm \cdot g^{-1}$, respectively. The above result indicates moderate $CaCO_3$ content can effectively regulate BET surface area. The above result can be further conformed by the pore size distribution in Fig. 1e. It is significant that PSNC-0.8 display more mesoporous and micropore structure than other samples. The rich mesoporous and micropore structure can provide fast O_2 diffusion transfer paths and more electrode/ electrolyte interface to fully explore catalytic sites, which all in favour of the ORR/OER catalytic activity.

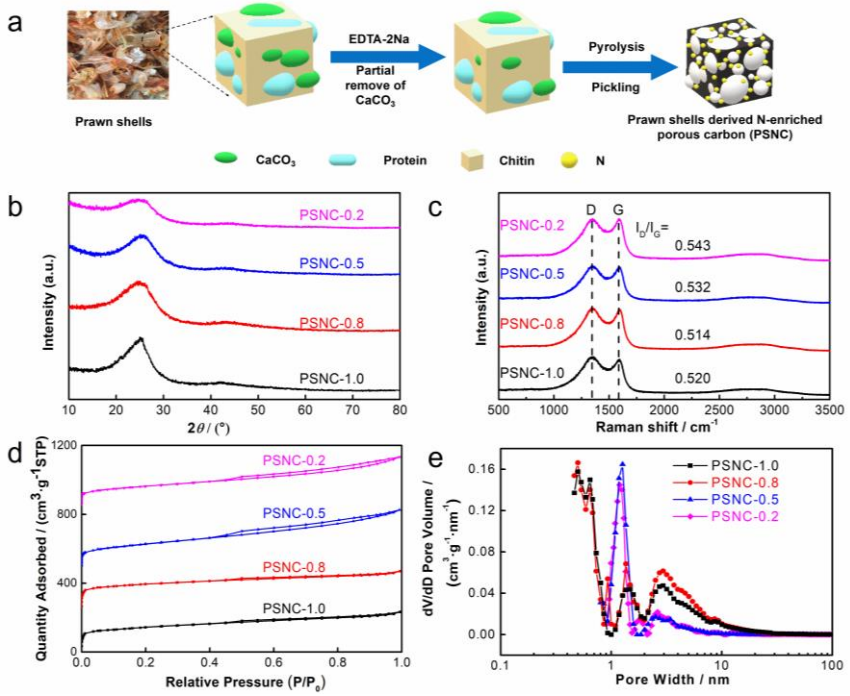

Fig. 1 a Schematic synthesis process of PSNC; **b** XRD, **c** Raman spectra, **d** N_2 adsorption-desorption isotherm and **e** pore size distribution of all PSNC samples

In addition, XPS was also conducted to analyse the surface chemical structure of PSNC samples. As anticipated, only C 1s, N 1s and O 1s peaks are observed in the full XPS spectrum (Fig. 2a), and the content of N in PSNC samples is almost same with a high value of ~8.30% (Table S2). The presence of O (Fig. S1a) can be largely attributed to physic-chemical adsorption between porous carbon material and some oxygen species [42]. From Fig. 2b, N 1s spectra can be fitted in three peaks, which are

corresponding to pyridinic N (398.5 eV), pyrrolic-N (400.4 eV) and graphitic-N (401.5 eV) [43,44]. Note that pyridinic-N and graphitic-N play an important part in constructing catalytic active sites [45,46]. Further analysis has revealed that the percentage of pyridinic-N and graphitic-N is closely related to with the content of $CaCO_3$ (Table S2). PSNC-0.8 possesses a high amount of pyridinic-N and graphitic-N (55.92%), while the value for PSNC-1.0, PSNC-0.5 and PSNC-0.2 is only 49.68%, 40.37% and 38.65%, respectively. Ingeniously, the specific surface area and pore size distribution also have the same variation tendency (Fig. 1c, d). The above results have enlightened that the pyridinic-N and pyrrolic-N may be precisely regulated by the formation process of pore structure. Besides, in C 1s spectrum (Fig. 2c), the subpeak at 286.5 eV is related to C-N bond, further confirmed the carbon matrix is doped by N atoms [42].

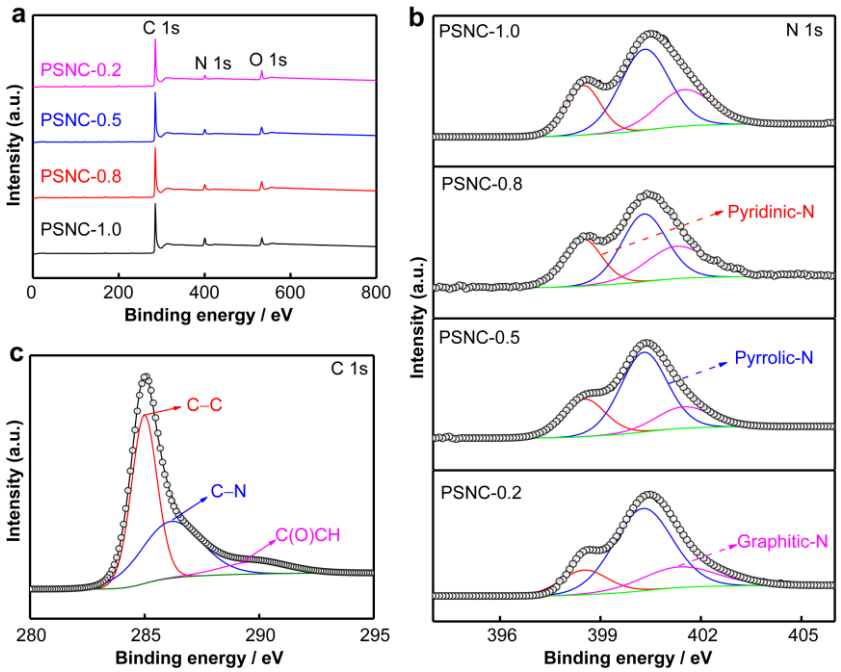

Fig. 2 a XPS survey spectrum and **b** N 1s for PSNC samples; **c** C 1s for PSNC-0.8

The morphological and structural characteristics of PSNC-0.8 are further investigated by SEM and TEM. In Fig. 3a-e, typical SEM and TEM images display that PSNC-0.8 delivers a continuous macro-meso-micropores frame structure, connected by the closely parked N-doping carbon nanoparticles. The above porous frame structure is beneficial for O_2 transport and electrolyte diffusion, as well as exposes more electrocatalytic active sites. Meanwhile, EDX elemental mapping further confirms the N-doping nature (Fig. 3f). Benefiting from continuous macro-meso-micropores structure and uniform N doping nature, the PSNC-0.8 is believed to deliver well oxygen electrocatalytic property.

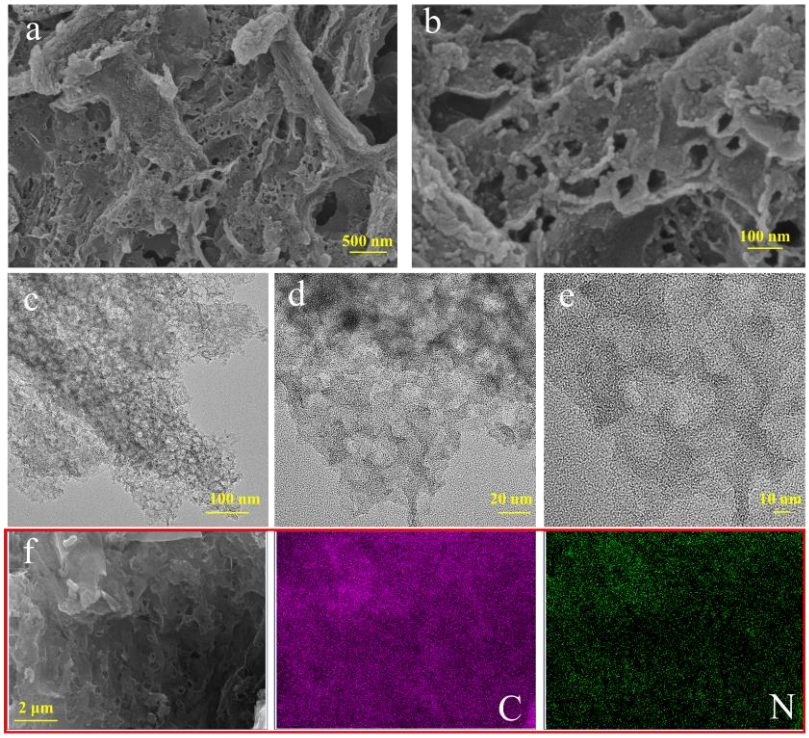

Fig. 3 a, b SEM, **c-e** TEM images, and **f** EDX elemental mapping of PSNC-0.8

3.2 Electrocatalytic property of ORR and OER

From CV tests in Fig. S2a,b, compared with N_2 atmosphere, a well-defined cathodic reduction peak is observed in O_2-saturated electrolyte, and the corresponding peak potential increases first and then reduces as the content of $CaCO_3$ increases. PSNC-0.8 achieves the most positive peak potential of 0.78 V with the best ORR activity. In addition, a same tendency is also presented in LSV tests. As shown in Fig. 4a, PSNC-0.8 displays a high onset potential (0.95 V) and half-wave potential ($E_{1/2}$=0.80 V) with the best ORR performance in all PSNC samples. And these values are even very close to those of Pt/C (0.96 and 0.805 V). Meanwhile, from the Tafel plots in Fig. 4b, PSNC-0.8 delivers the minimal Tafel slope of 62.7 mV·dec^{-1}, suggesting a faster catalytic reaction kinetics occurring in the surface of catalytic material, further demonstrating the superior ORR performance of PSNC-0.8. Besides, with the rotating rate from 400 to 2500 r·min^{-1}, the rise of current density rate implies a first-order reaction to ORR for PSNC-0.8 (Fig. 4c). From Koutecky-Levich (*K-L*)plots in Fig. 4d, the average electron transfer number is calculated to 3.78-3.86, indicating a well four-electron selectivity for PSNC-0.8. Furthermore, *i-t* chronoamperometric measurement was conducted at 0.80 V to assess ORR catalytic durability. After 12,000 s test period, the initial ORR current density retention for PSNC-0.8 and Pt/C is 85.61% and 72.48%, respectively (Fig. S2c), indicating PSNC-0.8 have an excellent ORR stability.

In addition to ORR performance, OER property were also evaluated with RuO_2 as the benchmark (Fig.4e). Ordinarily, the potential at 10 mA cm^{-2} ($E_{j=10}$) is often as the key parameter to estimate the OER activity. PSNC-0.8 displays a small $E_{j=10}$ of 1.60 V, which is more negative than that of PSNC-1.0 (1.63 V), PSNC-0.5 (1.65 V), PSNC-0.2 (1.67 V) and RuO_2 (1.605 V). The results have demonstrated that PSNC-0.8 also shows an excellent OER performance. Moreover, from *i-t* chronoamperometric measurement at 1.60 V (Fig. S2d), PSNC-0.8 achieves a more OER catalytic stability than RuO_2 (84.76% vs 74.75%). The potential gap ($\Delta E=E_{j=10}-E_{1/2}$) is an essential parameter to measure bifunctional electrocatalytic activity of a catalyst. A smaller ΔE value signifies a better bifunctional electrocatalytic activity. Clearly, PSNC-0.8 exhibits the minimum ΔE value of 0.80 V (Fig. 4f), which is also superior to most of reported carbon

based bifunctional electrocatalysts [38, 40, 47-52] (Fig. 4g). The excellent bifunctional electrocatalytic activity of PSNC-0.8 can be largely attributed to the synergistic effect of interconnected macro-meso-micropores structure to shorten O_2, electrolyte transmission pathway, and high amount of pyridinic-N and graphitic-N to provide abundant catalytic active sites as well as improve electron transfer (Fig. S1b).

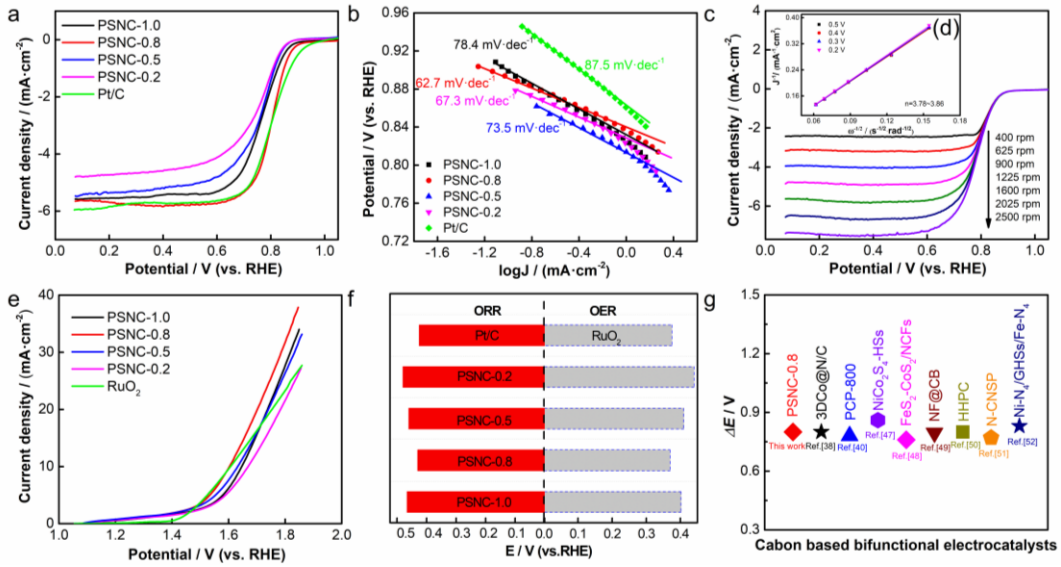

Fig. 4 a ORR polarization curves of PSNC samples and Pt/C; **b** Tafel plots derived from **a**; **c** ORR polarization curves of PSNC-0.8 from 400-2500 r·min^{-1}. **d** K-L plots at 0.2-0.5 V; **e** OER polarization profiles of PSNC samples and RuO_2; **f** overpotential differences between $E_{1/2}$ and $E_{j=10}$ of PSNC samples, Pt/C and RuO_2. **g** ΔE value of recently reported carbon-containing electrocatalysts and PSNC-0.8

3.3 RZAB performance of PSNC-0.8

A home-made RZAB is assembled to further confirm the electrocatalytic property of PSNC-0.8 (Fig. 5a). As shown in Fig. 5b, the open circuit voltage for PSNC-0.8 is 1.49 V, which is 20 mV positive than Pt/C+RuO_2 (1.47 V). In addition, from the discharge-charge curves and power density plots in Fig. 5c, PSNC-0.8 delivers a large current density of 351.2 mA·cm^{-2} at 0.5 V, and the corresponding peak power density is about 176.5 mW·cm^{-2}. For comparison, a weaken electrochemical property (222 mA·cm^{-2} and 110.3 mW·cm^{-2}) is presented by Pt/C+RuO_2. Meanwhile, PSNC-0.8 exhibits a narrow charge-discharge voltage gab, indicating that PSNC-0.8 possesses a fast transfer rate for charge and oxygen species during the charge-discharge process. From the discharge curves in Fig. 5d, PSNC-0.8 achieves a stable discharge platform of 1.21 V. Calculating by Zn consumption, the specific discharge capacity for PSNC-0.8 is about 781.9 mAh·g_{Zn}^{-1}. To Pt/C+RuO_2, the discharge platform and specific capacity is only 1.20 V and 778.5 mAh·g_{Zn}^{-1}, respectively. More importantly, from the long-term cyclic life in Fig. 5e, PSNC-0.8 displays an excellent cycle stability. After continued running for 320 h (480 cycles), the decay of battery efficiency is only 6.5%, and the voltage gap increasing is about 0.13 V. In contrast, the voltage gap increasing for Pt/C+RuO_2 is over 1.20 V only after 308 cycles. Additionally, the cycle property of PSNC-0.8 also surpasses other most recently reported RZAB (Table S3). The long-term cycling test results further demonstrates the superior ORR and OER catalytic activity for PSNC-0.8.

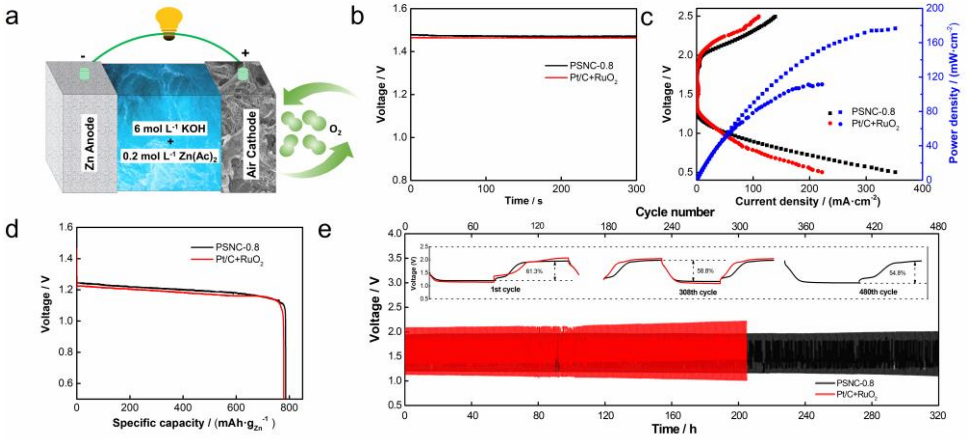

Fig. 5 a scheme of a RZAB; **b** open circuit voltage plots of different cathode catalyst based RZAB; **c** charge-discharge polarization curves and corresponding power density plots; **d** discharge curves at 10 mA·cm^{-2}; **e** galvanostatic long-term cycling test at 10 mA·cm^{-2} with 20 min discharge and 20 min charge

4 Conclusion

In conclusion, a prawn shells derived N-enriched porous carbon has been successfully synthesized by an ion exchange coupled biomimetic mineral self-sacrificing template assisted strategy. The optimized PSNC-0.8 delivers an outstanding ORR and OER catalytic activity with a small ΔE of 0.80 V. Meanwhile, PSNC-0.8 based RZAB presents a satisfactory long-term cycle stability with a low voltage gap increasing of 0.13 V after 480 cycles. The superior ORR/OER performance of PSNC-0.8 are largely put down to synergistic effect of interconnected macro-meso-micropores structure and high content of pyridinic and graphitic nitrogen, including abundant catalytic active sites and shortening charge and mass transfer pathway. This work inspires a simple and effective conception to design metal-free electrocatalysts for rechargeable metal-air battery, and also expands a new way for high value application of seafood waste.

Acknowledgments This study was financially supported by the Innovative Youth Talents of Guangdong Education Department Support Program (No. 2021KQNCX027), the Youth Innovative Talents Project of Zhanjiang (No. 2021E05016) and the Program for Scientific Research Start-Up Funds of Guangdong Ocean University (Nos. 060302122010 and R19047).

Declarations

Conflict of interests The authors declare that they have no conflict of interest.

References

[1] Wang TT, Wang PY, Pang YJ, Wu YT, Yang J, Chen H, Gao XR, Mu SC, Kou ZK. Vertically mounting molybdenum disulfide nanosheets on dimolybdenum carbide nanomeshes enables efficient hydrogen evolution. Nano Res. 2022; 15(5): 3946. https://doi.org/10.1007/s12274-022-4072-5.

[2] Li LL, Yu DS, Li P, Huang HJ, Xie DY, Lin CC, Hu F, Chen HY, Peng SJ. Interfacial electronic coupling of ultrathin transition-metal hydroxide nanosheets with layered MXenes as a new prototype for platinum-like hydrogen evolution. Energ Environ Sci. 2021; 14(12): 6419. https://doi.org/10.1039/D1EE02538D.

[3] Deng LM, Hu F, Ma MY, Huang SC, Xiong YX, Chen HY, Li LL, Peng SJ. Electronic modulation caused by interfacial Ni-O-M (M= Ru, Ir, Pd) bonding for accelerating hydrogen evolution kinetics. Angew Chem Int Edit. 2021; 133(41): 22450. https://doi.org/10.1002/ange.202110374.

[4] Sui YL, Zhou J, Wang XW, Wu L, Zhong SK, Li YG. Recent advances in black-phosphorus-based materials for electrochemical energy storage. Mater Today. 2021; 42:117. https://doi.org/10.1016/j.mattod.2020.09.005.

[5] Wang ZY, Jiang SD, Duan CQ, Wang D, Luo SH, Liu YG. In situ synthesis of Co_3O_4 nanoparticles confined in 3D

nitrogen-doped porous carbon as an efficient bifunctional oxygen electrocatalyst. Rare Met. 2020;39(12):1383.https://doi.org/10.1007/s12598-020-01581-4.

[6] Qu XY, Huang H, Wan T, Hu L, Yu ZL, Liu YJ, Dou A, Zhou Y, Su MR, Peng XQ, Wu TH, Wu T, Chu DW. An integrated surface coating strategy to enhance the electrochemical performance of nickel-rich layered cathodes. Nano Energy. 2022; 91:106665. https://doi.org/10.1016/j.nanoen.2021.106665.

[7] Liu ZS, Li LJ, Chen J, Yang HP, Xia LF, Chen JX, Duan JF, Chen ZY. Effects of chelating agents on electrochemical properties of $Na_{0.9}Ni_{0.45}Mn_{0.55}O_2$ cathode materials. J Alloys Compd. 2021; 855: 157485. https://doi.org/10.1016/j.jallcom.2020.157485.

[8] Zhang L, Zhu JW, Li X, Mu SC, Verpoort F, Xue JM, Kou ZK, Wang J. Nurturing the marriages of single atoms with atomic clusters and nanoparticles for better heterogeneous electrocatalysis. Interdiscip Mater. 2022;1(1): 51. https://doi.org/10.1002/idm2.12011.

[9] Wang TT, Wang PY, Zang WJ, Li X, Chen D, Kou ZK, Mu SC, Wang J. Nanoframes of Co_3O_4-Mo_2N heterointerfaces enable high-performance bifunctionality toward both electrocatalytic HER and OER. Adv Funct Mater. 2022; 32(7): 2107382. https://doi.org/10.1002/adfm.202107382.

[10] Hu F, Yu DS, Ye M, Wang H, Hao YN, Wang LQ, Li LL, Han XP, Peng SJ. Lattice-matching formed mesoporous transition metal oxide heterostructures advance water splitting by active Fe-O-Cu bridges. Adv Energy Mater. 2022; 12(19): 2200067.https://doi.org/10.1002/aenm.202200067.

[11] Wang CY, Yang CH, Zhang ZC.Unraveling molecular-level mechanisms of reactive facet of carbon nitride single crystals photocatalyzing overall water splitting. Rare Met. 2020;39(12):1353 .https://doi.org/10.1007/s12598-020-01568-1.

[12] Leong KW, Wang YF, Ni M, Pan WD, Luo SJ, Leung, DYC. Rechargeable Zn-air batteries: Recent trends and future perspectives. Renew Sust Energ Rev. 2022; 154: 111771. https://doi.org/10.1016/j.rser.2021.111771.

[13] Yao CC, Li JX, Zhang ZH, Gou CL, Zhang ZS, Pan G, Zhang J. Hierarchical core-shell Co_2N/CoP embedded in N, P-doped carbon nanotubes as efficient oxygen reduction reaction catalysts for Zn-air batteries, Small. 2022; 18: 2108094. https://doi.org/10.1002/smll.202108094.

[14] Xiao X, Hu XY, Liang Y, Zhang GL, Wang XY, Yan YC, Li XH, Yan GC, Wang JX. Anchoring $NiCo_2O_4$ nanowhiskers in biomass-derived porous carbon as superior oxygen electrocatalyst for rechargeable Zn-air battery. J. Power Sources. 2020; 476: 228684. https://doi.org/10.1016/j.jpowsour.2020.228684.

[15] Logeshwaran N, Ramakrishnan S, Chandrasekaran SS, Vinothkannan M, Kim AR, Sengodan S, Velusamy DB, Varadhan P, He JH, Yoo DJ. An efficient and durable trifunctional electrocatalyst for zinc–air batteries driven overall water splitting. Appl Catal B-Environ. 2021; 297:120405. https://doi.org/10.1016/j.apcatb.2021.120405.

[16] Zhang L, Zhu YX, Nie ZC, Li ZY, Ye Y, Li LH, Hong J, Bi ZH, Zhou YT, Hu GZ. Co/MoC nanoparticles embedded in carbon nanoboxes as robust Trifunctional electrocatalysts for a Zn-air battery and water electrocatalysis. ACS nano. 2021; 15(8): 13399. https://doi.org/10.1021/acsnano.1c03766.

[17] Huang HJ, Yu DS, Hu F, Huang SC, Song JN, Chen HY, Li LL, Peng SJ. Clusters induced electron redistribution to tune oxygen reduction activity of transition metal single-atom for metal-air batteries. Angew Chem Int Edit. 2022; 134(12): e202116068. https://doi.org/10.1002/ange.202116068.

[18] Liu JL, Xiao JX, Wang ZY, Yuan HM, Lu ZG, Luo BC, Tian EK, Waterhouse GIN, Structural and electronic engineering of Ir-doped Ni-(oxy) hydroxide nanosheets for enhanced oxygen evolution activity. ACS Catal. 2021; 11(9): 5386. https://doi.org/10.1021/acscatal.1c00110.

[19] Lv D. Layered double hydroxides functionalized by carbonaceous materials: from preparation to energy and

environmental applications. Environ Sci Pollut R. 2022; 29: 30865–30891. https://doi.org/10.1007/s11356-021-18179-7.

[20] Guo YM，Zhang LJ，XiLi DG，Kang J. Advances of carbon materials as loaders for transition metal oxygen/sulfide anode materials. Chin J Rare Met. 2021;45(10):1241-1257. https://doi.org/10.13373/j.cnki.cjrm.XY20040016.

[21] Wang P, Wang T, Qin R, Pu ZH, Zhang CT, Zhu JW, Chen D, Kou ZK, Mu SC, Wang J. Swapping catalytic active sites from cationic Ni to anionic S in nickel sulfide enables more efficient alkaline hydrogen generation. Adv Energy Mater. 2022; 12(8): 2103359. https://doi.org/10.1002/aenm.202103359.

[22] Song JN, Qiu SY, Hu F, Ding YH, Han SL, Li LL, Chen HY, Han XP, Sun CH, Peng SJ. Sub-2 nm thiophosphate nanosheets with heteroatom doping for enhanced oxygen electrocatalysis. Adv Funct Mater. 2021; 31(19): 2100618. https://doi.org/10.1002/adfm.202100618.

[23] Arafat Y, Azhar MR, Zhong YJ, Tadé MO, Shao ZP. Metal-free carbon based air electrodes for Zn-air batteries: Recent advances and perspective. Mater Res Bull. 2021; 140: 111315. https://doi.org/10.1016/j.materresbull.2021.111315.

[24] Yu DS, Zhang Q, Dai LM. Highly efficient metal-free growth of nitrogen-doped single-walled carbon nanotubes on plasma-etched substrates for oxygen reduction. J Am Chem Soc. 2010; 132(43): 15127. https://doi.org/10.1021/ja105617z.

[25] Niu J, Shao R, Liu MY, Zan YX, Dou ML, Liu JJ, Zhang ZP, Huang YQ, Wang F. Porous carbons derived from collagen‐enriched biomass: Tailored design, synthesis, and application in electrochemical energy storage and conversion. Adv Funct Mater. 2019; 29(46): 1905095. https://doi.org/10.1002/adfm.201905095.

[26] Wang Y, Qiao MF, Mamat X. Nitrogen-doped macro-meso-micro hierarchical ordered porous carbon derived from ZIF-8 for boosting supercapacitor performance. Appl Surf Sci. 2021; 540: 148352. https://doi.org/10.1016/j.apsusc.2020.148352.

[27] Wang Z, Cheng D, Chen C, Zhou KB. Hierarchically porous carbon microspheres with fully open and interconnected super-macropores for air cathodes of Zn-air batteries. Carbon. 2018, 136: 54. https://doi.org/10.1016/j.carbon.2018.04.061.

[28] Doustkhah E, Hassandoost R, Khataee A, Luque R, Assadi MHN, Hard-templated metal-organic frameworks for advanced applications. Chem Soc Rev. 2021; 50(5): 2927. https://doi.org/10.1039/C9CS00813F.

[29] Wang H, Shao Y, Mei SL, Lu Y, Zhang M, Sun JK, Matyjaszewski K, Antonietti M, Yuan JY. Polymer-derived heteroatom-doped porous carbon materials. Chem Rev. 2020; 120(17): 9363. https://doi.org/10.1021/acs.chemrev.0c00080.

[30] Wang D, Xu H, Yang PX, Xiao LH, Du L, Lu XY, Li RP, Zhang JQ, An MZ. A dual-template strategy to engineer hierarchically porous Fe-N-C electrocatalysts for the high-performance cathodes of Zn-air batteries. J Mater Chem A. 2021; 9(15):9761. https://doi.org/10.1039/D1TA00585E.

[31] Zhang L, Jin L, Liu B, He J. Templated growth of crystalline mesoporous materials: from soft/hard templates to colloidal templates. Front Chem. 2019, 7: 22. https://doi.org/10.3389/fchem.2019.00022.

[32] Wang G, Sun YH, Li DB, Liang HW, Dong RH, Feng XL, Müllen K. Controlled synthesis of N-doped carbon nanospheres with tailored mesopores through self-assembly of colloidal silica. Angew Chem. 2015; 127(50): 15406. https://doi.org/10.1002/ange.201507735.

[33] Campbell J, Abnett J, Kastania G, Volodkin D, Vikulina AS. Which biopolymers are better for the fabrication of multilayer capsules? A comparative study using vaterite $CaCO_3$ as templates. ACS Appl Mater Inter. 2021; 13(2): 3259. https://doi.org/10.1021/acsami.0c21194.

[34] Mondal AK, Kretschmer K, Zhao YF, Liu H, Fan HB, Wang GX. Naturally nitrogen doped porous carbon derived from waste shrimp shells for high-performance lithium ion batteries and supercapacitors. Micropor Mesopor Mat. 2017; 246: 72. https://doi.org/10.1016/j.micromeso.2017.03.019.

[35] Xiao X, Zhang WZ, Zhao H, Li LF, Deng PC, Wu YL, Luo SL, Chen BB. Ultrathin amorphous MnO_2 modified prawn shells-derived porous carbon towards robust oxygen electrocatalyst for rechargeable Zn-air battery. Ceram Int. 2022;

48(5): 6506. https://doi.org/10.1016/j.ceramint.2021.11.195.

[36] Gao F, Zang YH, Wang Y, Guan CQ, Qu JY, Wu MB. A review of the synthesis of carbon materials for energy storage from biomass and coal/heavy oil waste. New Carbon Mater. 2021, 36(1): 34. https://doi.org/10.1016/S1872-5805(21)60003-3.

[37] Mathew GM, Sukumaran RK, Sindhu R, Binod P, Pandey AJ. Green remediation of the potential hazardous shellfish wastes generated from the processing industries and their bioprospecting. Environ Technol Inno. 2021; 24: 101979. https://doi.org/10.1016/j.eti.2021.101979.

[38] Han MN, Shi MJ, Wang J, Zhang ML, Yan C, Jiang JT, Guo SH, Sun ZY, Guo ZH. Efficient bifunctional Co/N dual-doped carbon electrocatalysts for oxygen reduction and evolution reaction. Carbon. 2019; 153: 575. https://doi.org/10.1016/j.carbon.2019.07.075.

[39] Wu Z, Yuan L, Han QR, Lan YJ, Zhou Y, Jiang XH, Ouyang XP, Zhu JW, Wang X, Fu YS. Phosphorous/oxygen co-doped mesoporous carbon bowls as sulfur host for high performance lithium-sulfur batteries. J Power Sources. 2020; 450: 227658. https://doi.org/10.1016/j.jpowsour.2019.227658.

[40] Shi XJ, He BB, Zhao L, Gong YS, Wang R, Wang HW. FeS2-CoS2 incorporated into nitrogen-doped carbon nanofibers to boost oxygen electrocatalysis for durable rechargeable Zn-air batteries. J Power Sources. 2021; 482: 228955. https://doi.org/10.1016/j.jpowsour.2020.228955.

[41] Jiang H, Wang YQ, Hao JY, Liu YS, Li WZ, Li J. N and P co-functionalized three-dimensional porous carbon networks as efficient metal-free electrocatalysts for oxygen reduction reaction. Carbon. 2017; 122: 64. https://doi.org/10.1016/j.carbon.2017.06.043.

[42] Li LH, Song L, Guo H, Xia W, Jiang C, Gao B, Wu C, Wang T, He JP. N-Doped porous carbon nanosheets decorated with graphitized carbon layer encapsulated Co_9S_8 nanoparticles: an efficient bifunctional electrocatalyst for the OER and ORR. Nanoscale. 2019; 11(3): 901. https://doi.org/10.1039/C8NR07179A.

[43] Hu CG, Dai LM. Doping of carbon materials for metal‐free electrocatalysis. Adv Mater. 2019; 31(7): 1804672. https://doi.org/10.1002/adma.201804672.

[44] Xu DY, Long XD, Xiao JX, Zhang ZL, Liu GY, Tong HX, Liu Z, Li N, Qian D, Li JH, Li JL. Rationally constructing CoO and $CoSe_2$ hybrid with CNTs-graphene for impressively enhanced oxygen evolution and DFT calculations. Chem Eng J. 2021; 422: 129982. https://doi.org/10.1016/j.cej.2021.129982.

[45] Cui HJ, Jiao MG, Chen YN, Guo YB, Yang LP, Xie ZJ, Zhou Z, Guo SJ. Molten-salt-assisted synthesis of 3D holey N-doped graphene as bifunctional electrocatalysts for rechargeable Zn-air batteries. Small Methods. 2018; 2(10): 1800144. https://doi.org/10.1002/smtd.201800144.

[46] Zhang XR, Wang YQ, Wang K, Huang YL, DD. Lyu, Yu F, Wang SB, Tian ZQ, Shen PK, Jiang SP. Active sites engineering via tuning configuration between graphitic-N and thiophenic-S dopants in one-step synthesized graphene nanosheets for efficient water-cycled electrocatalysis. Chem Eng J. 2021; 416: 129096. https://doi.org/10.1016/j.cej.2021.129096.

[47] Ji HP, Wang MF, Liu SS, Sun H, Liu J, Qian T, Yan CL. Pyridinic and graphitic nitrogen-enriched carbon paper as a highly active bifunctional catalyst for Zn-air batteries. Electrochim Acta. 2020; 334: 135562. https://doi.org/10.1016/j.electacta.2019.135562.

[48] Feng XT, Jiao QZ, Cui HR, Yin MM, Li Q, Zhao Y, Li HS, Zhou W, Feng CH. One-pot synthesis of $NiCo_2S_4$ hollow spheres via sequential ion-exchange as an enhanced oxygen bifunctional electrocatalyst in alkaline solution. ACS Appl Mater Inter. 2018; 10(35): 29521. https://doi.org/10.1021/acsami.8b08547.

[49] Zhu P, Gao JX, Chen XW, Liu S. An efficient metal-free bifunctional oxygen electrocatalyst of carbon co-doped with

fluorine and nitrogen atoms for rechargeable Zn-air battery. Int J Hydrogen Energ. 2020; 45(16): 9512. https://doi.org/10.1016/j.ijhydene.2020.01.131.

[50] Xiao X, Li XH, Wang ZX, Yan GC, Guo HJ, Hu QY, Li LJ, Liu Y, Wang JX. Robust template-activator cooperated pyrolysis enabling hierarchically porous honeycombed defective carbon as highly-efficient metal-free bifunctional electrocatalyst for Zn-air batteries. Appl Catal B-Environ. 2020; 265: 118603. https://doi.org/10.1016/j.apcatb.2020.118603.

[51] Zong LB, Wu WC, Liu SL, Yin HJ, Chen YN, Liu C, Fan KC, Zhao XX, Chen X, Wang FM, Yang Y, Wang L, Feng SH. Metal-free, active nitrogen-enriched, efficient bifunctional oxygen electrocatalyst for ultrastable zinc-air batteries. Energy Storage Mater. 2020; 27: 514. https://doi.org/10.1016/j.ensm.2019.12.013.

[52] Wang W, Liu YC, Li J, Luo J, Fu L, Chen SL. NiFe LDH nanodots anchored on 3D macro/mesoporous carbon as a high-performance ORR/OER bifunctional electrocatalyst. J Mater Chem A. 2018; 6(29): 14299. https://doi.org/10.1039/C8TA05295F.